Hindawi Publishing Corporation
International Journal of Photoenergy
Volume 2016, Article ID 2947510, 14 pages
http://dx.doi.org/10.1155/2016/2947510

Research Article

Synthesis of CdS Sensitized TiO_2 Photocatalysts: Methylene Blue Adsorption and Enhanced Photocatalytic Activities

A. B. Makama,[1] A. Salmiaton,[1] E. B. Saion,[2] T. S. Y. Choong,[1] and N. Abdullah[1]

[1]*Department of Chemical and Environmental Engineering, Universiti Putra Malaysia (UPM), 43400 Serdang, Selangor, Malaysia*
[2]*Department of Physics, Universiti Putra Malaysia (UPM), 43400 Serdang, Selangor, Malaysia*

Correspondence should be addressed to A. B. Makama; abmakama@hotmail.com

Received 10 December 2015; Accepted 24 January 2016

Academic Editor: Wanjun Wang

A series of CdS/TiO_2 nanocomposites with different Cd to Ti molar ratio were synthesized from P25-TiO_2 nanopowder using microwave-assisted hydrothermal method. The as-produced powders were characterized by XRD, electron microscopy, EDX, and UV-Vis diffuse reflectance spectroscopy. The adsorption capacity and photocatalytic activity of the samples were investigated using methylene blue as a model pollutant. Sorption tests revealed that the adsorption of MB onto the samples obeys the Freundlich-Langmuir isotherm model. The sorption capacity decreased as follows: TiO_2 > TCd2 > TCd1 > TCd3 > TCd4. The results of the photocatalytic tests under high-intensity discharge (HID) lamp revealed that CdS/TiO_2 powders with low Cd to Ti molar ratios exhibited much higher activities than P25-TiO_2. The CdS/TiO_2 sample with 20% CdS/(TCd2) showed the most activity among all these samples. The results also show that the Cd to Ti molar ratio of the nanocomposite has a significant effect on the photodegradation of MB and the enhanced activities exhibited by the nanocomposites are because of the low rate of electron-hole recombination.

1. Introduction

Conventional dye abatement strategies based on physicochemical process and fluid mechanics have been argued to be effective [1, 2]. However, questions remain on the cost and future sustainability of these techniques. Also it had been argued that the methods transfer the pollutants from water bodies to sludge or to other solid systems thereby necessitating the need for secondary remediation steps [3, 4]. Similarly, conventional aerobic and anaerobic bioremediation processes such as enzymatic catalysis [1] are generally considered less effective because microorganisms do not use the colored constituents of organic dyes as foods, and thus, the dyes remain largely unaffected [5]. This state of affairs has led to the search for more efficient and cost-effective methods capable of transforming the organic dyes into environmentally benign products.

Existing studies [6–8] have revealed that semiconductor photocatalysis is a potentially viable process capable of complete mineralization of dyes to benign substances. Photocatalysis is a complex multistep process that involves [9] (a) photogeneration of charge carriers ($e^- + h^+$), (b) separation, recombination, and transport of the carriers to the photocatalyst's surface, and (c) surface redox reaction. The reductive and oxidative surface reactions involve the transfer of electrons and holes to preadsorbed reactants. The rates of these reactions depend on the efficiency and rate of charge transfer between the photocatalyst and the substrate. This, in turn, depends on the type of linkage between the photocatalysts and adsorbate. A strong and specific link (adsorption) results in direct charge transfer which induced higher photocatalytic activity. On the other hand, a weak substrate adsorption leads to indirect charge transfer and low photocatalytic activity [10].

Among the semiconductors under investigation, TiO_2 is considered the standard because it is relatively cheap, nontoxic, and chemically stable [11]. Furthermore, upon photoexcitation with UV light, it produces highly oxidizing holes (+2.53 eV versus standard hydrogen electrode (SHE)) and reducing electrons (−0.52 eV/SHE) capable of generating H_2O_2, $^{\bullet}OH$ radical, and superoxide O_2^-, which play important roles in photodegradation [12]. Unfortunately however,

Table 1: Different types of pollutant degraded by CdS/TiO_2 based photocatalysts.

Nanocomposite	Light	Pollutant	Reference
CdS/TiO_2	SSL[a]	MB[b]	[14]
CdS/TiO_2-ACF[c]	SL[d]	MB	[19]
CNT[e]/CdS-TiO_2	UV & Vis	MB	[20]
CdS-[f]C60/TiO_2	US[g]	RhB[h]	[21]
TNTA[i]/CdS	Vis	MO[j]	[22]
CdS-TiO_2	Vis	EtOH gas	[23]
CdS/TiO_2	Vis	RhB & MO	[24]
CdS/TiO_2	Vis	RhB & 4-CP[k]	[25]

[a]Simulated solar light. [b]Methylene blue. [c]Activated carbon fiber. [d]Sunlight. [e]Carbon nanotube. [f]Buckyball. [g]Ultrasonic irradiation. [h]Rhodamine B. [i]TiO_2 nanotube array. [j]Methylene orange. [k]4-Chlorophenol.

pristine TiO_2 is only photoactive when irradiated with radiation from the ultraviolet region whose wavelength, λ, is $\leq$ 387.5 nm because of its large band gap. This constraint limits the utilization of terrestrial solar radiation by TiO_2 to about 3%–5%. In order to utilize more terrestrial solar energy and improve the usefulness of TiO_2, it is thus imperative to extend its photoactivity to the visible light region.

Towards the above end, many strategies [13] have been developed to extending the activity of TiO_2 to the visible light region. These strategies include compounding with a visible light active semiconductor with more negative cathodic potential than TiO_2 [14, 15] such as CdS. The CdS/TiO_2 nanocomposite configuration has attracted a great deal of interest because of the positions of their band gaps edges relative to each other. Variant forms of the CdS/TiO_2 nanocomposite have been investigated as visible light photocatalyst for splitting of water [16–18] and degradation of natural pollutants. Table 1 lists some of the CdS/TiO_2 based photocatalysts used in pollution abatement.

One of the methods of preparing CdS sensitized TiO_2 under mild operating conditions is microwave-assisted nanomaterial synthesis method. The method has several advantages, including rapid and uniform heating throughout the entire liquid volume which reduces reaction time and offers the potential for higher control over nucleation and crystal growth [26]. In this paper, a series of CdS sensitized TiO_2 nanocomposites with different Cd : Ti molar ratio content (0.1–0.4) were synthesized via microwave-assisted hydrothermal method. The influence of CdS content on the physicochemical, optical, adsorption, and photocatalytic properties of the composites was investigated.

The goals of this study are therefore to (a) synthesize and characterize a series of CdS/TiO_2 nanocomposite photocatalysts with different Cd : Ti molar content from P25-TiO_2 using a low-power hydrothermal microwave-assisted method, (b) investigate the effects of Cd : Ti content on the adsorption capacities of the samples from batch studies and adsorption kinetics, and (c) determine and compare the rates of photocatalytic degradation of an organic dye (methylene blue) over the different photocatalysts under high-intensity discharge (HID) lamp illumination.

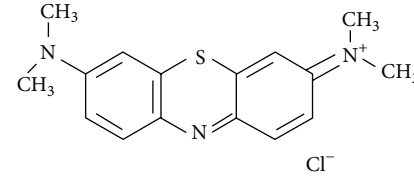

Scheme 1: Structural formula of methylene blue dye.

2. Materials and Methods

2.1. Materials. Titanium dioxide nanopowder (TiO_2, Aldrich), cadmium chloride ($CdCl_2 \cdot 2.5H_2O$, QRec), ammonium chloride (NH_4Cl 99.8%, R&M Chemicals), sodium hydroxide pellets (NaOH, Emsure), and thiourea, ($(NH_2)_2CS$, >99%, Merck) were procured and used as received without further purification. Similarly, methylene blue ($C_{16}H_{18}N_3SCl$, ≥82%, Sigma Aldrich), a member of the thiazine dye class (Scheme 1), was purchased and used as a substrate to evaluate the adsorptive capacities and photoactivities of the samples. All solutions and dispersions were produced with 18.2 MΩ·cm distilled deionized water.

2.2. Synthesis of CdS Sensitized TiO_2 Photocatalysts. In a typical process, 0.5 g (6.3 mmol) of TiO_2 core is dispersed in 100 mL of 5.3 mmol L^{-1} $CdCl_2 \cdot 2.5H_2O$ solution by sonication at 50% amplitude and a pulsed regime of 30 s on and 2 s off for 10 min. 100 mL of 1 mole/L NH_4Cl solution and 50 mL 10.6×10^{-3} moles/L solution of thiourea (Tu) were added to the above mixture and stirred with a magnetic stirrer for 10 min. The pH was adjusted to about 10 using 1 mole/L solution of NaOH. The final colloidal solution (~350 mL) was irradiated continuously at 20% power (180 W) for 20 min in a microwave (MW) oven. The irradiated mixture was allowed to cool to room temperature overnight and the precipitate was removed and purified in 4 cycles of centrifugation and washing with DI water and absolute ethanol. This product is designated TCd1. Similarly, other photocatalysts with different starting Cd : Ti molar ratios of 0.2 : 1, 0.3 : 1, and 0.4 : 1 were synthesized and designated TCd2, TCd3, and TCd4, respectively. In all syntheses processes, a constant 1 : 2 molar ratio of cadmium chloride and thiourea was used relative to the Cd : Ti molar ratio.

2.3. Characterization. The crystallinity and the phase structure of the samples were investigated using Phillips Analytical X-ray diffractometer. The measurements were carried out with $Cu_{K\text{-}\alpha}$ radiation between 2θ values of 20°–80° at a scan rate of $0.033^\circ s^{-1}$ using accelerating voltage and current of 40 mV and 40 mA, respectively. The morphological structures and the finer structural details of the samples were viewed and photographed with Joel Schottky field-emission scanning electron microscope (FE-SEM) model JSM-7600F and Hitachi H-7100 STEM transmission electron microscope (TEM). Chemical composition of the nanocomposites was determined with energy-dispersive X-ray spectrometry (EDS) analysis also taken on the same machine. Ultraviolet-visible (UV-Vis) diffuse reflectance spectra were obtained

with a Shimadzu UV-3600 UV-Vis-NIR spectrophotometer equipped with a $BaSO_4$ coated integrating sphere. The reflectance measurements (R_{sample}) were converted to equivalent absorption spectra using the so-called Kubelka-Munk function $F(R_\infty)$ (1) for an infinitely thick sample [27]:

$$F(R_\infty) = \frac{(1 - R_\infty)^2}{2R_\infty}, \quad (1)$$

where

$$R_\infty = \frac{R_{sample}}{R_{BaSO_4}}. \quad (2)$$

In the region near the absorption edge, the energy dependence of the absorption coefficient (α) for semiconductors is given by the classical [28] relationship:

$$\alpha E_p = K\left(E_p - E_{bg}\right)^n, \quad (3)$$

where E_p is photon energy in eV (= 1239.7/λ, λ is the radiation wavelength, nm), E_{bg} is the band gap, K is a constant, and n is also a constant whose value depends on the nature of the optical transition (caused by photon absorption) and also on the crystal structure of the semiconductor. In crystalline semiconductors, where crystal momentum is conserved and electron transitions adhere strictly to the selection (or transition) rules, n has the value of 1/2, 3/2, 2, and 3 when the transitions are direct-allowed, direct-forbidden, indirect-allowed, and indirect-forbidden, respectively [29]. On the other hand, in amorphous, homogenous semiconductors, where the momentum vector is not conserved, the value of n is 2 irrespective of the type of transition found in crystalline materials of the same composition.

2.4. Adsorption Studies. Five aluminum foil wrapped stopper conical flasks of 50 mL capacity were used in the batch adsorption experiments. 0.05 g of the photoadsorbent is added to each of the flasks containing 25 mL of MB solutions having concentrations of 10 mg L^{-1}, 8 mg L^{-1}, 6 mg L^{-1}, 4 mg L^{-1}, and 2 mg L^{-1}, respectively. After adding the catalysts, the flasks were agitated in a thermostatic shaker at 150 rpm and 300.0±0.3 K for 2 h. Immediately after, 2 mL aliquot was taken from each flask and centrifuged at 5,000 rpm for 5 min and the remaining MB content in the supernatant was determined spectrophotometrically by reading the absorbance values at 664 nm. Equilibrium data for the CdS/TiO_2 composite adsorbents were generated using this procedure. Kinetics data were also obtained in similar manner but with aliquots taken at 20 min intervals for a maximum of 2 h. The two sets of data on amount of MB adsorbed at equilibrium (Q_e, mg/g) and with time (Q_t), mg/g in each flask, were calculated with [30]

$$Q_e = \frac{(C_0 - C_e)V}{m_{cat}}, \quad (4)$$

$$Q_t = \frac{(C_0 - C_t)V}{m_{cat}}, \quad (5)$$

where C_0, C_e, and C_t represent the initial concentration, concentrations at equilibrium, and concentration at time t of MB (mg/L), respectively. m_{cat} is the mass of the photocatalysts adsorbent used in flask (g), and V is the volume (L) of adsorbate (MB) solution in the flask.

2.5. Photocatalytic Activity Measurement. Photocatalytic activities of the catalysts' systems were investigated by degradation of MB experiments. In a typical run, 0.10 g CdS/TiO_2 nanocomposite was added to 250 mL MB solution (10 mg L^{-1}). The solution was stirred in the dark for 30 min (based on adsorption-time experiments) to establish adsorption/desorption equilibrium. Subsequently, photocatalytic degradation of MB was initiated by exposing the mixture to white light irradiation from six xenon high-intensity discharge (HID) lamps (4300 K) of 35 W each at room temperature and atmospheric pressure. The lamps were located 10 cm from the surface of the mixture. Aliquots of about 3 mL were drawn from the photoreactor at 20 min intervals and quickly centrifuged at 5,000 rpm for 5 min to separate the catalyst particles. The decolorization of MB was monitored by recording the spectrum of each supernatant between the 500 nm to 750 nm range on a Shimadzu UV-1800 spectrophotometer. The absorbance of each supernatant at the 664 nm characteristic absorption peak was converted to concentration using MB standard calibration curve. P25-TiO_2 photocatalyst was adopted as the reference for comparison of the photocatalytic activity of the CdS/TiO_2 nanocomposites under the same experimental conditions.

3. Results and Discussion

3.1. Characterization of Photocatalysts

3.1.1. X-Ray Diffraction. The crystallite phases of the synthesized CdS/TiO_2 samples were investigated using powder X-ray diffraction (PXRD) measurements. Figure 1 shows the PXRD diffractograms obtained and the reference stick patterns of bulk anatase TiO_2 and greenockite (hexagonal) phase CdS. All the nanocomposites' diffractograms show prominent peaks at 2θ positions of 25.3°, 37.8°, 48.2°, 54.1°, and 55.1° attributed to the (101), (004), (200), (105), and (211) planes of bulk anatase TiO_2 that matches ICDD card number 21-1272. In addition to the TiO_2 peaks, the diffractograms of TCd3 and TCd4 samples show new peaks at ≈27.0°, 28.7°, 37.1°, 48.2°, and 51.2°. These peaks are indexed to reflections from the (002), (101), (102), (110), and (112) planes of hexagonal CdS according to ICDD card number 01-7112. The CdS peaks were not visible on the TCd1 and TCd2 diffractograms. The absence of the CdS peaks is probably because the amount CdS on these samples is less than the lower limit of detection [31]. The observed evolutionary trend of the CdS peaks with increased loading on TiO_2 is consistent with similar reports in the literature [32, 33]. The broadening of the prominent peaks indicates that the samples consist of nanosized crystals.

3.1.2. Electron Microscopy and EDX Analyses. The samples morphological and structural details were obtained with

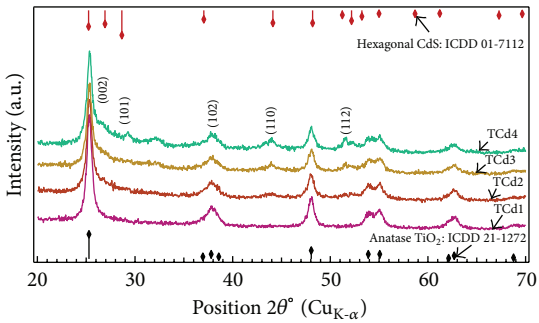

Figure 1: Powder XRD patterns of the TiO_2-CdS photocatalysts systems. Standard diffraction (stick) patterns of bulk anatase TiO_2 (bottom black) and bulk hexagonal CdS (top red) are shown as references.

field-emission scanning electron spectroscopy (FESEM). Figure 2(a) shows the loosely bound agglomerates of the commercial TiO_2 nanoparticles of approximately (37.2 ± 7.9) nm length and (15.3 ± 2.1) nm diameter. In Figures 2(b)–2(e), the effects of CdS compounding on the TiO_2 surface morphology and particles are shown. After CdS loading, all the resulting nanocomposite samples consist of cemented rough surfaced agglomerates. The high-surface energy of nanoparticles is known to cause particles agglomeration [34]. However, in the present study, the severe levels of agglomeration and cementation observed can also be attributed in part to the precipitation of CdS on the surfaces and interstitial spaces of the TiO_2 particles.

Figure 3 shows the finer structural details of the TiO_2 and nanocomposite samples. Careful analyses of images of the nanocomposites (Figures 3(b)–3(d)) indicate that the samples consist of nanoparticles of semispherical particles in various stages of development.

The particle size of the samples increased as the Cd : Ti molar ratio increased indicating that more CdS is deposited on the TiO_2. Figure 4 depicts the shifts of the Gaussian fits to the size distribution histograms from left to right as the Cd : Ti ratio increase. Sample TCd1 shows the narrowest size distribution while TCd3 exhibits the widest. The particle sizes to one standard deviation of TCd1, TCd2, TCd3, and TCd4 were estimated to be 6.5 ± 0.1 nm, 21.1 ± 0.8 nm, 27.3 ± 1.5 nm, and 34.3 ± 0.4 nm, respectively.

The EDX elemental content (wt.%) of the synthesized CdS/TiO_2 composites is listed in Table 2. The result shows that the nanocomposites consist of Ti, O, Cd, and S, which further confirms the presence of CdS in the samples. The Cd and S content in the nanocomposites increased as the Cd : Ti molar ratio increased. Figure 5 shows the typical EDX spectrum of TCd sample.

3.1.3. UV-Visible Analysis. Figure 6 shows the UV-Vis diffuse reflectance (DR) spectra of pure TiO_2 and those of the synthesized TCdX (X = 1–4) nanocomposites. The TiO_2 spectrum shows only one strong absorption in the ultraviolet region (dotted region A) but no absorption in the visible region (dotted region B). This is because of wide band gap of

Table 2: Elemental compositions and band gaps of the as-synthesized CdS/TiO_2 photocatalysts.

Sample	Elements, wt.%					E_{bg}
	Cd : Ti	Ti (K)	O (K)	Cd (L)	S (K)	
TiO_2	0	20.81	79.19	—	—	3.35
TCd1	0.1 : 1	12.58	43.76	1.57	0.10	3.10
TCd2	0.2 : 1	4.86	26.85	1.51	0.23	3.00
TCd3	0.3 : 1	9.65	35.93	3.51	0.67	2.80
TCd4	0.4 : 1	7.45	32.25	5.85	0.86	2.70

TiO_2 which makes it active only in UV light. On the other hand, the spectra of the TCdX (X = 1–4) systems show overlap of the spectra coming from the titania (i.e., 330 nm–390 nm) and the CdS (i.e., 400 nm–600 nm). This result corroborates the findings of [23, 33], and others on similar systems. The figure also shows that with increasing Cd : Ti molar ratio (i.e., CdS loading), the absorption edges of the nanocomposites shift towards longer wavelengths. The band gaps of the samples were estimated using the Tauc plot shown on the inset of Figure 6 and itemized in Table 2. The band gaps of the nanocomposites TCd1, TCd2, TCd3, and TCd4 red shifted by −0.25 eV, −0.34 eV, −0.55 eV, and −0.65 eV compared to the band gap (3.35 eV) of TiO_2. This observation is in line with the typical behavior of reverse type-1 nanocomposite semiconductor systems [35] and similar result has been reported by [36]. Collectively, the findings outlined above confirm the successful syntheses of visible light photoactive CdS/TiO_2 nanocomposites.

3.2. Adsorption and Photocatalysis of Methylene Blue

3.2.1. Adsorption Isotherms. Figure 7 shows a plot of measured sorption data of MB on to the parent TiO_2 and the nanocomposites. Profiles of the isotherms appear to obey the Langmuir model or the Freundlich model. Thus, to determine the model that best describes the sorption of MB by the adsorbents, the experimental data were analyzed using Langmuir (6), Freundlich (7), and Freundlich-Langmuir (Sips) (8) models. The nonlinear forms of these equations are expressed as [37]

$$Q_e = \frac{Q_0 b_L C_e}{1 + b_L C_e}. \quad (6)$$

The terms Q_e and C_e are as defined in (4). Q_0 is the maximum monolayer adsorption capacity of the adsorbent and b_L represents the Langmuir bonding constant related to the energy of adsorption:

$$Q_e = K_F C_e^{1/n}, \quad (7)$$

where K_F (mg/g(L/mg)$^{1/n}$) and n are the Freundlich constants characteristics to the system. These parameters indicate a measure of the adsorption capacity of the sorbent and favorability of the adsorption process, respectively:

$$Q_e = \frac{Q_0 K_S C_e^{1/n}}{1 + K_S C_e^{1/n}}, \quad (8)$$

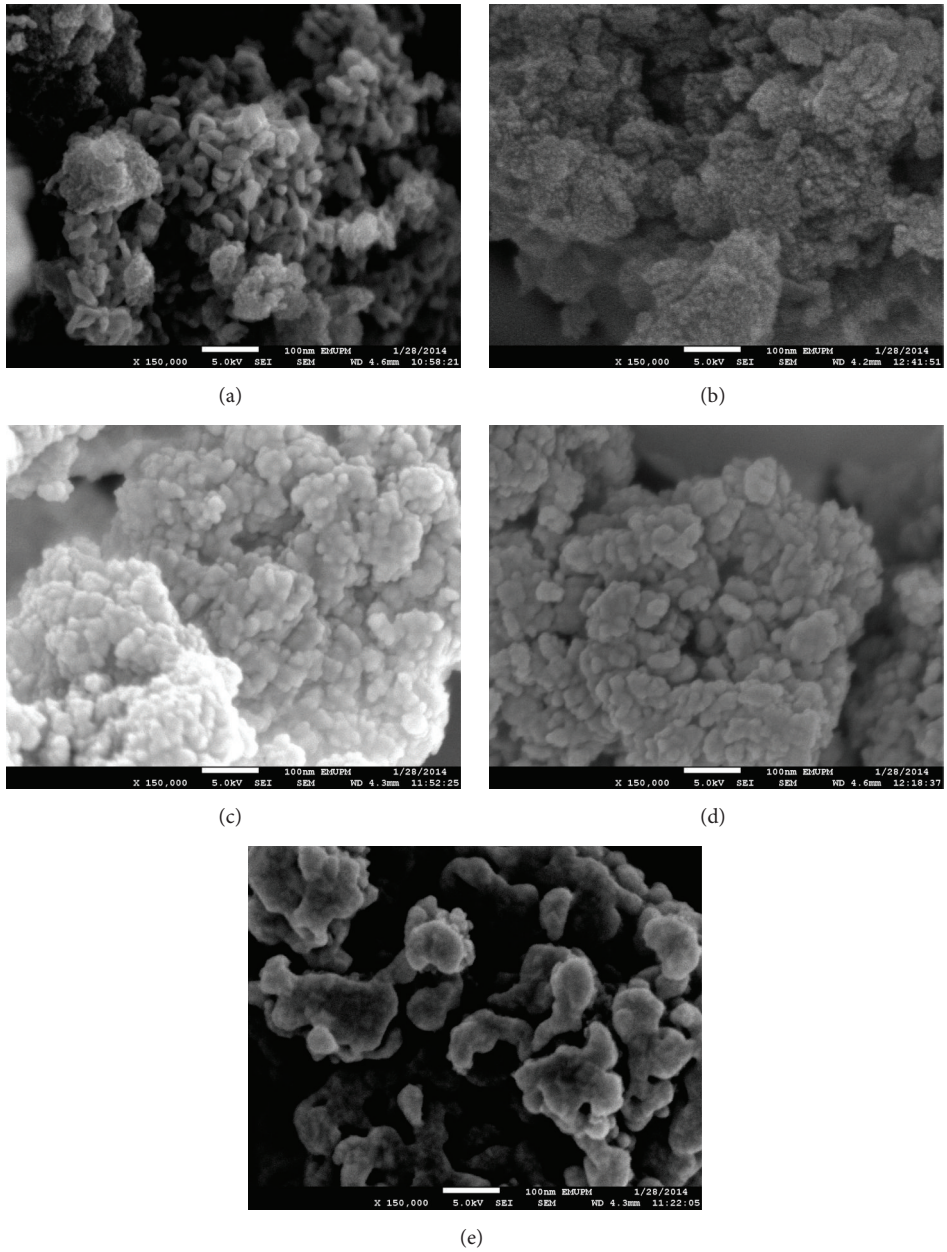

Figure 2: FESEM images of (a) TiO_2 particles, (b) TCd1, (c) TCd2, (d) TCd3, and (e) TCd4 nanocomposites taken at 150K magnification and 5.0 kV SEI signal. Scale bar 100 nm.

where K_S and n are the Sips equilibrium constant (L/g) and isotherm model exponent, respectively.

Experimental data are fitted to the nonlinear model equations using IGOR Pro v6.34A (WaveMetrics, Inc., Lake Oswego, Oregon, USA). Chi-square (χ^2) goodness-of-fit test was used to select the model that best describes the sorption process.

The nonlinear fits of sorption data obtained with the different models are shown in Figures 7(b)–7(d). From the figures, it appears that all the three sorption models described the experimental data reasonably well. However, analysis of the fitting parameters and values of the goodness-of-fit (χ^2) for the models as summarized in Table 3 present a different picture. Values of the separation factor (R_L) of the Langmuir model and the heterogeneity factor ($1/n$) of Freundlich model for all samples lie between 0 and 1 indicating thermodynamically favorable adsorption [38]. The Freundlich model predicted much lower adsorption capacities (K_F) for the sorbents compared to the experimental value and returned the biggest χ^2 error values indicating that it does not satisfactorily describe the sorption of MB by the samples. In contrast, the maximum monolayer capacities (Q_0) predicted by Langmuir and Sips models show good agreement with experimental values and much smaller χ^2 values. The better fitting and good

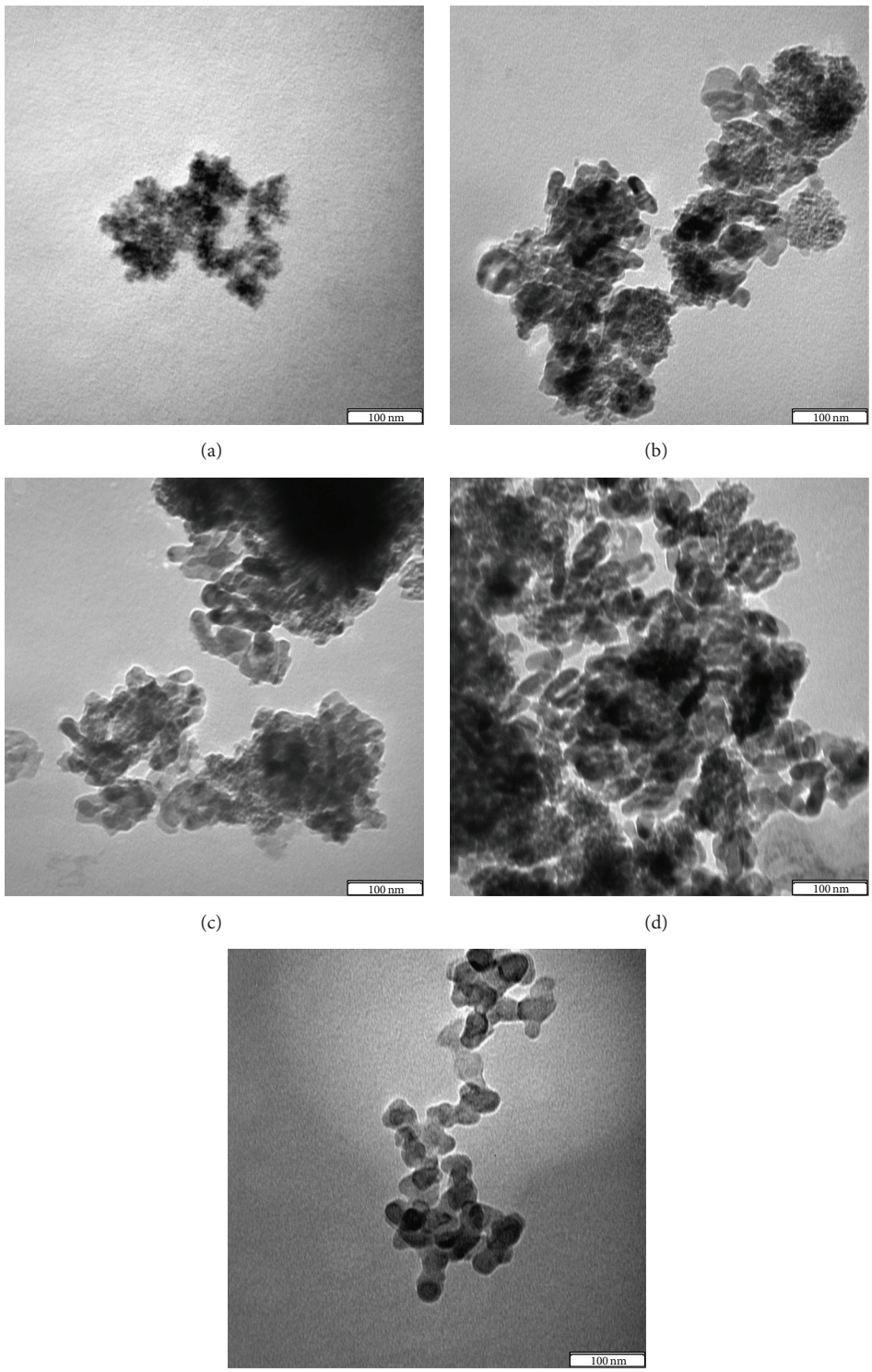

Figure 3: TEM images of (a) TiO_2 particles, (b) TCd1, (c) TCd2, (d) TCd3, and (e) TCd4 nanocomposites taken at 200K magnification. Scale bar 100 nm.

Table 3: Nonlinear Langmuir, Freundlich, and Sips constants for MB adsorption on different adsorbents obtained from the NL fits shown in Figures 7(b)–7(d).

Isotherm model	Samples				
	TiO_2	TCd1	TCd2	TCd3	TCd4
Langmuir					
Q_0, mg MB/g cat.	14.3	14.9	12.0	8.2	7.8
b_L, L/mg MB	0.125	0.030	0.070	0.037	0.035
R_L	0.10	0.25	0.13	0.21	0.22
χ^2	0.987	0.099	0.120	0.052	0.010
Freundlich					
K_F, mg MB/g (L/mg MB)$^{1/n}$	4.669	1.315	2.574	1.051	0.931
$1/n$	0.25	0.48	0.32	0.41	0.42
χ^2	4.138	0.554	0.418	0.076	0.087
Freundlich-Langmuir (Sips)					
Q_0, mg MB/g	13.1	14.9	13.3	10.7	8.7
K_S, L/g	0.054	0.030	0.092	0.053	0.043
n	0.689	1.000	1.210	1.340	1.148
χ^2	0.535	0.099	0.082	0.022	0.003
SSA, $m^2\ g^{-1}$	29.6	33.7	30.0	24.2	19.6

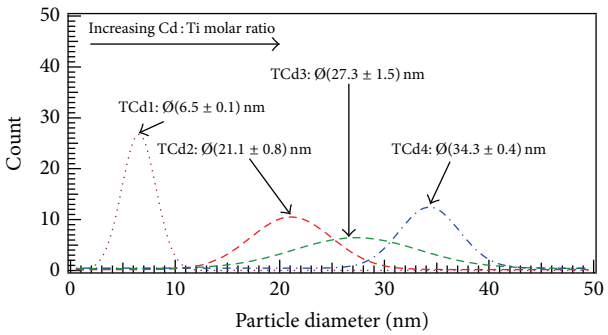

Figure 4: Evolution of particle size with increase in Cd : Ti molar ratio.

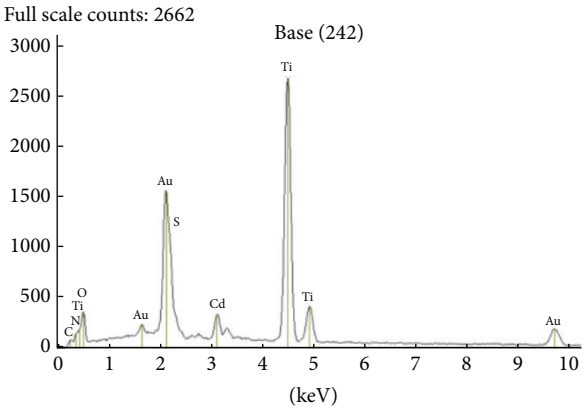

Figure 5: Representative EDX spectrum of TCd4 nanocomposite.

correlation obtained with these models indicate that they are adequate representations of MB sorption by the samples. Based on the chi-square test criterion, the Sips model is the

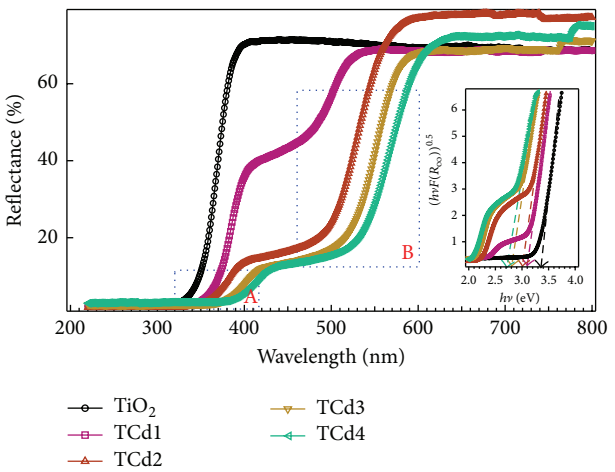

Figure 6: Room temperature UV-Visible diffuse reflectance spectra of the parent TiO_2 and the TCdX (X = 1 to 4) nanocomposite photocatalyst. Inset is the Tauc plots of $(h\nu F(R_\infty))^{0.5}$ versus $h\nu$ showing the band gaps of the titania core and the core-shell systems.

better model because it produces better fitting parameters for all the system except for TCd1. For the TCd1 sample, both Langmuir and Sips models predicted same model constants because the Sips model reduces to Langmuir model since exponential constant (n) in (8) is one. Thus, the Sips model reduces to Langmuir equation. In literature, several authors have reported Langmuir-type adsorption behavior for MB dye on different adsorbents. Some of these adsorbents included bamboo-based activated carbon [39], P25-titania [40], TiO_2 nanotubes [41], and Fe_2O_3-activated carbons [42]. The in this work is probably due to the compounding of TiO_2 with CdS which might have altered the surface chemistry of the adsorbent.

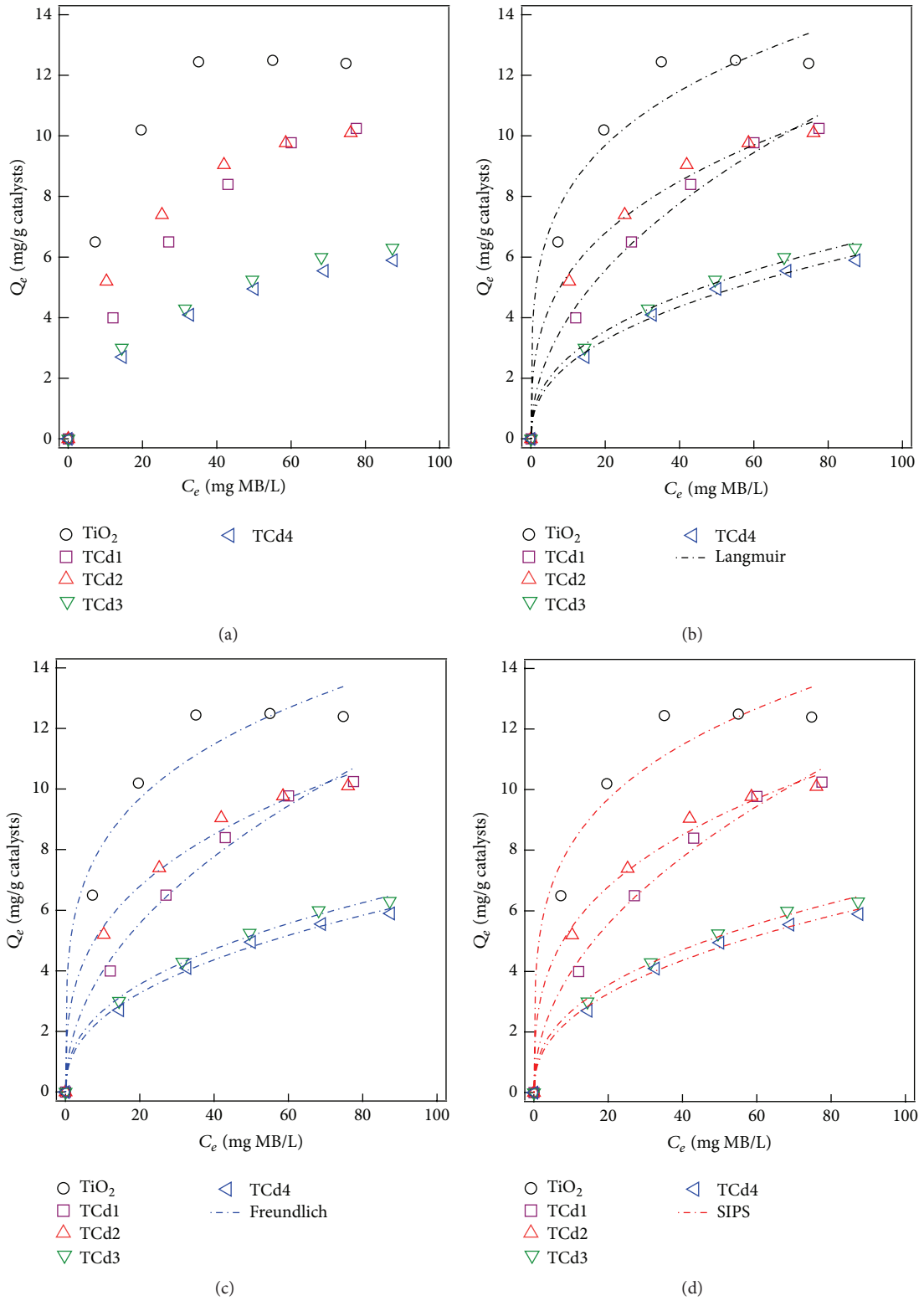

FIGURE 7: (a) Profile of MB sorbed as a function of equilibrium concentration for the different adsorbents. Other panels show nonlinear fit of experimental data from (a) to (b) Langmuir, (c) Freundlich, and (d) Freundlich-Langmuir model equations. Experimental conditions: pH = 7.44 and T = (300.0 + 0.3) K and initial MB adsorbate concentration, C_0 = 100.0 mg L^{-1}.

Table 4: Comparison of the pseudo-first-order, pseudo-second-order adsorption rate constants and calculated and experimental Q_e values obtained at 100 mg/L MB concentration for the different photoadsorbents.

Sample	$Q_{e,\exp}$ [a]	Pseudo-first-order kinetics			Pseudo-first-order kinetics		
		k_1 [b]	$Q_{e,\text{cal}}$ [a]	χ^2	k_2 [c]	$Q_{e,\text{cal}}$ [a]	χ^2
TiO_2	12.6	0.0789	12.0	0.862	0.0115	13.0	0.529
TCd1	10.5	0.0631	10.2	2.315	0.0088	11.3	1.225
TCd2	12.0	0.0787	11.2	0.753	0.0121	12.1	0.197
TCd3	6.5	0.0499	5.9	0.264	0.0100	6.8	0.186
TCd4	6.3	0.0647	5.6	0.655	0.0167	6.2	0.419

[a] $Q_{e,\exp}$ and $Q_{e,\text{cal}}$ have units of mg/g; [b] k_1 has units of min^{-1}; [c] k_2 has units of g $(\text{mg min})^{-1}$.

3.2.2. Adsorption Kinetics. The nonlinear forms of Lagergren's pseudo-first-order rate (LPFO) [43] (9) and the pseudo-second-order (PSO) [44] (10) kinetic models were used to investigate the effect of time on sorption of MB by the adsorbents:

$$Q_t = Q_0 \left[1 - \exp\left(-kt\right)\right], \tag{9}$$

$$Q_t = \frac{k_2 Q_e^2 t}{1 + k_2 Q_e k}, \tag{10}$$

where Q_t is as earlier defined in (4). k_1 (min^{-1}) and k_2 $(\text{g}(\text{mg min})^{-1})$ are first-order and second-order rate constants, respectively, and t (min) is contact time.

Figure 8(a) shows the MB concentration profiles with time during the dark absorption process for the different adsorbents. The profiles indicate that the initial adsorption of MB onto the different adsorbents is fast. For all adsorbents, over 80% of the adsorption capacity was reached within the first 20 min of adsorption. Similar quick initial uptake of MB on other adsorbents has been reported in the literature [41, 45]. At equilibrium, more MB is adsorbed by titania than by any of the synthesized nanocomposites as shown in Figures 8(b) and 8(c) and listed in Table 4. This relatively high absorptive capacity of TiO_2 can be attributed to its smaller particle size compared to those of the nanocomposites. The deposition/coating of CdS on the surface of TiO_2 causes the sizes of the resulting nanocomposites to be bigger than those of the parent TiO_2 (Figure 4) which results in decreased sorption capacities for the nanocomposites [46].

The predicted maximum adsorption capacity ($Q_{e,\text{cal}}$) and rate constants k_1 and k_2 from the NLFs of the experimental data LPFO and PSO kinetic models are listed in Table 4 together with their corresponding goodness-of-fit (χ^2) values. The PSO kinetics model shows better fitting of data (smaller χ^2 values) than the LPFO model. Also, the adsorption capacities ($Q_{e,\text{cal}}$) predicted by PSO show better agreement with experimental data ($Q_{e,\text{exp}}$) as shown in Table 4. Therefore, the PSO model approximates the adsorption reaction more satisfactorily indicating a chemisorption process.

3.2.3. Photocatalytic Degradation. The white section of Figure 9(a) shows the variation of MB adsorbate concentration with irradiation time over the different photocatalysts. From this graph, it is evident that about 3 times more MB is removed by photocatalysis process than by adsorption (darkened section of the graph).

Table 5: Kinetics parameters and photocatalytic degradation efficiency (η) of MB achieved over the different CdS/TiO_2.

Sample	k_a, min^{-1}	χ^2	η, [%]	$k_a/k_{r\text{TiO}_2}$	$t^{0.5}$, min
TiO_2	0.0030	0.0002	30.0	1.0	231
TCd1	0.0128	0.0013	79.6	4.3	55
TCd2	0.0165	0.0007	85.9	5.3	42
TCd3	0.0050	0.0018	46.8	1.7	142
TCd4	0.0049	0.0023	40.1	1.3	173

According to earlier experimental results [47, 48], the photocatalytic degradation of MB obeys the heterogeneous pseudo-first-order Langmuir-Hinshelwood (LH) model given as

$$r = -\frac{dC}{dt} = \frac{k_r K_e C}{1 + K_e C}, \tag{11}$$

where r represents the initial rate of photocatalytic degradation (mg min^{-1}), C the concentration of the reactant (mg L^{-1}), t the irradiation time (min), k_r the rate constant of the reaction $(\text{mg L}^{-1}\ \text{min}^{-1})$, and K_e the adsorption coefficient of the reactant (L mg^{-1}). At low concentrations ($C \ll 1$) [49], (11) can be simplified to the apparent rate order equation:

$$C_t = C_0 \exp\left(-k_a t\right), \tag{12}$$

where k_a $(= k_r K_e)$ is the apparent first-order rate constant and C_0 is the initial concentration of the MB pollutant. The rate constants, k_a, are determined by nonlinear regressing of experimental data as shown by the broken lines in Figure 9(a). The k_a determined are listed in Table 5, and it is apparent from their values that there is a marked improvement in the photocatalytic activities of the nanocomposites over that of TIO_2 under the current experimental conditions. In Column 6 of Table 5, ratios of $k_a/k_{r(\text{TiO}_2)}$ show that samples TCd1, TCd2, and TCd3 exhibit about 4, 5, and 2 times more activity than TiO_2. While TCd4 has about the same activity as TiO_2. These k_a values are in quantitative agreement with the reported findings of [19, 33] on similar photocatalysts' systems.

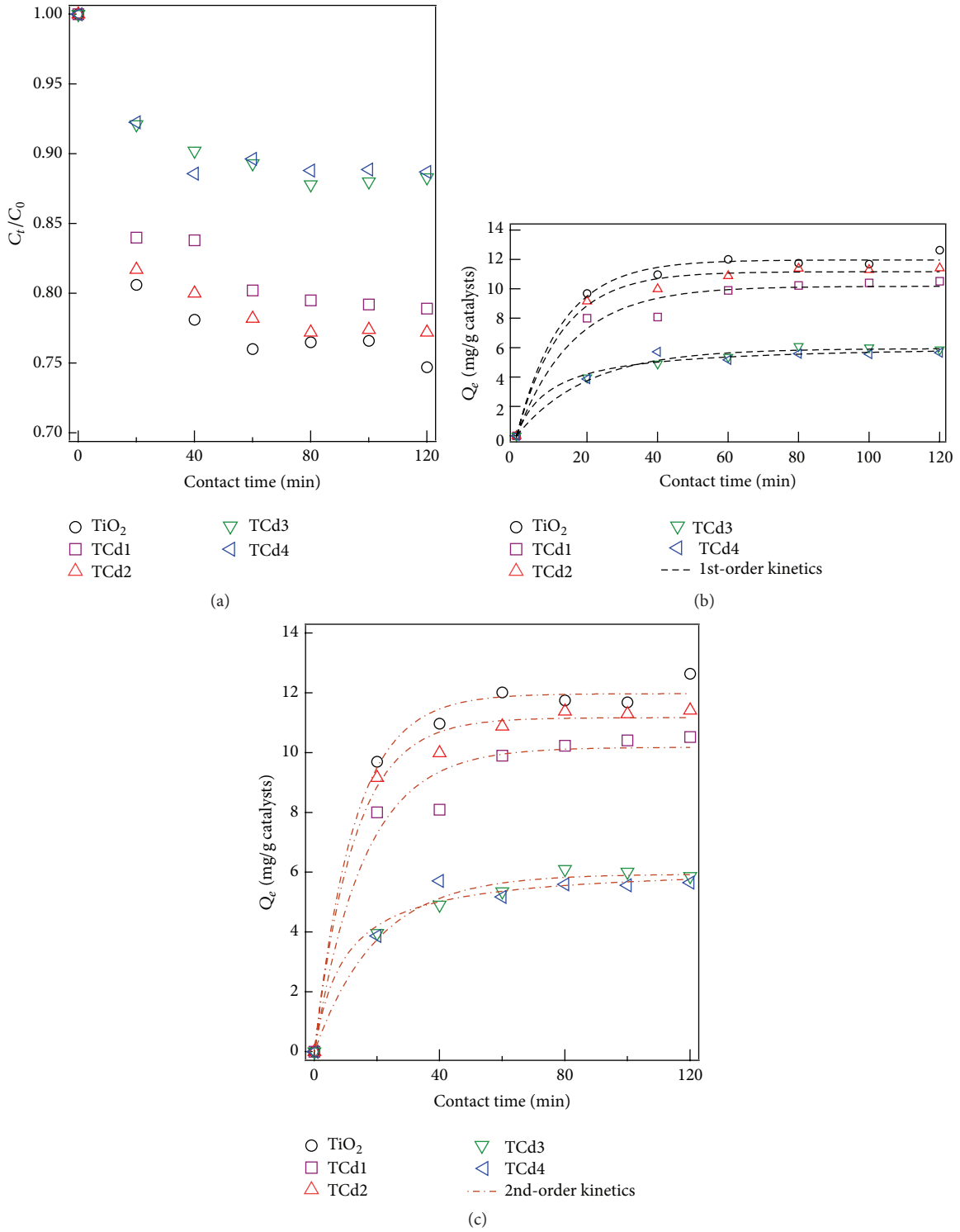

Figure 8: (a) Effect of contact time on the residual concentration of MB over the different adsorbents. Nonlinear fits of (b) pseudo-first-order and (c) pseudo-second-order kinetic models to the sorption time data for the various adsorbents at C_0 = 100 mg/L, pH = 7.44, and T = (300.0 ± 0.3) K.

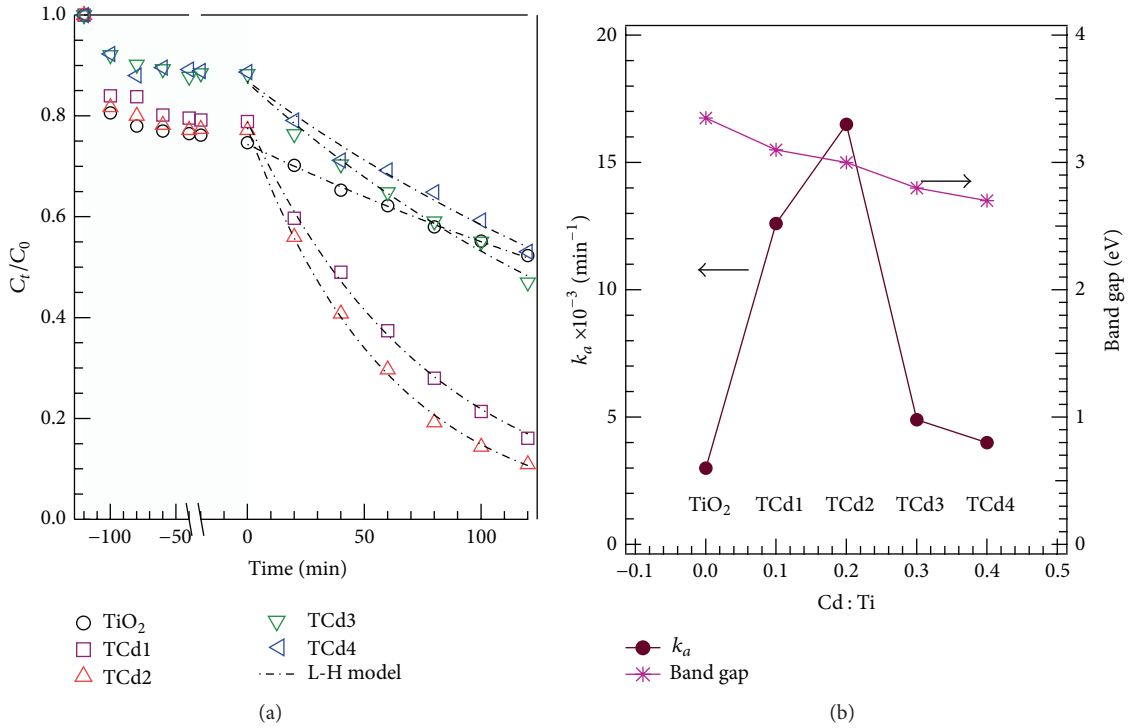

FIGURE 9: (a) Profiles of photocatalytic degradation of MB with time and NLF of experimental data to the apparent pseudo-first-order kinetics model over the different photocatalysts (white section). (b) Comparison of apparent rate constants k_a (blue plot) of photodegradation of MB with the band gaps (red plot) of the corresponding photocatalysts as a function of Cd : Ti molar ratio. Experimental conditions: 0.1 g catalysts, T = (300.0 + 0.3) K 35 W Xenon HID light irradiation.

Figure 9(b) shows a comparison between the apparent rate (k_a) of photodegradation of MB by the different photocatalysts and their corresponding band gaps. The rate constant-molar ratio plot (blue) shows the variation of rate constant as a function of nominal Cd : Ti molar ratio. The plot shows k_a rose rapidly from 0.0030 min^{-1} at a molar ratio of 0 (i.e., the value for parent TiO_2) to the maximum rate of 0.0165 min^{-1} for TCd2 at molar ratio of 0.2. Thereafter, the rate falls sharply to 0.0049 min^{-1} with further increase in molar ratio to 0.3 and then tapers off to 0.0040 min^{-1} at a ratio of 0.4. Similar, rise and fall in the photocatalytic rate constants with CdS loading have been reported by [33].

The difference in photoactivity between TiO_2 and the nanocomposites is related to their respective band gaps. The TiO_2 sample is a wide band gap semiconductor (3.35 eV equivalent to 370 nm) that is most photoactive in UV light. Although the HID light source used in this experiment generates most of its radiation energy in the visible region between 405 nm and 475 nm, some amount of UV rays is also generated [50]. The UV rays activate the TiO_2 to generate some charge carriers that effect the degradation of MB. On the other hand, because the nanocomposites are active in visible light in addition to UV light, more charge carriers are generated by these samples that go to oxidize greater number of preadsorbed MB molecules. Secondly, as explained in detail under mechanism, there is more efficient charge carrier (e^-_{cb}–h^+_{vb}) separation and longer lifetimes in the nanocomposite samples which offers more opportunity for the redox reaction to occur than in the pure titania [20].

The thickness of a coat/or film on a particle has a profound effect on the electrochemical properties of the resulting composite [51, 52]. Above a certain critical thickness, high strain induced by constraint heteroepitaxy often leads to interfacial defects. The defects impede charge carrier separation and mobility because they serve as recombination centers and traps [53, 54]. This means that, as the density of interfacial defects increases with increasing film thickness, the nanocomposites became less electrochemically active as a result of high rates of charge carrier trapping and recombination. At high Cd : Ti molar ratio, more CdS precursors are available for growth. Accordingly, the probability of growing thick CdS coats on the surface of titania also increases. Consequently, nanocomposites with thick coats and more interfacial defects are produced thereby reducing their photoactivity. Another possible reason for the low-photoactivity of TCd3 and TCd4 is due to their large sizes 27.3 nm and 34.3 nm, respectively. Larger particle diameters mean the e^-_{cb}+ h^+_{vb} pairs have long distances to travel before reaching the particle-electrolyte interface. If the particle diameter d_p is greater than the mean free diffusion lengths, L_e and L_h of the e^-_{cb} and h^+_{vb}, respectively, it is then likely that carriers generated at the interior of particles may not reach the interface to

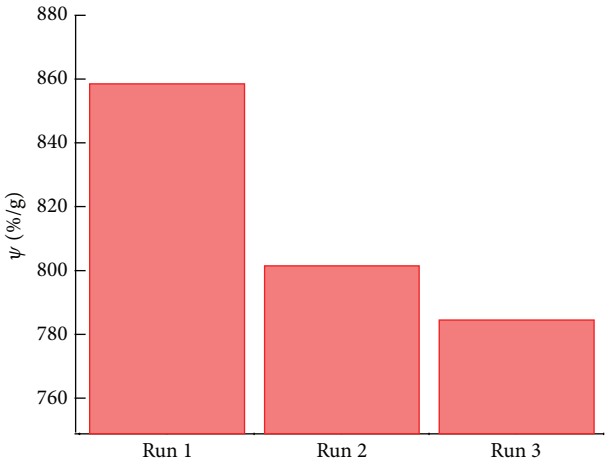

Figure 10: Cycling degradation curve for CdS-TiO_2 with 0.2 Cd : Ti molar ratio.

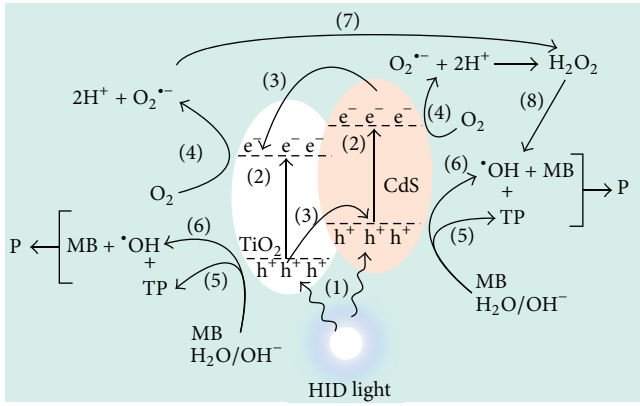

Figure 11: Scheme diagram of the photocatalytic reaction of MB on TiO_2/CdS.

partake in the redox reaction [53]. Furthermore, TCd3 and TCd4 have low-sorption for MB; as such, when the h^+_{vb} reach the surface, on few adsorbed molecules MB are present for reaction [33].

3.2.4. Stability of Photocatalyst. To evaluate the stability of the catalyst, recycling degradation tests were carried out on TCd2 using the procedure given in [55]. Three cycles of repeat experiments were done and the results of the tests are shown as bar of efficiency (η) per mass of catalyst in gram (ψ) versus number of test runs in Figure 10. TCd2 exhibits a good MB removal efficiency (85.9%) in the first run. The efficiency dropped by 56%/g in the second run and by 18%/g after the second run. It can be deduced that, under the present experimental conditions, TCd2 is a stable catalyst for degradation of MB. The cycling tests again confirm that CdS nanoparticles could be anchored on the mesoporous substrate effectively and stably via bifunctional groups.

3.3. Photocatalytic Degradation of MB Mechanism. The proposed mechanism of MB degradation over the nanocomposite photocatalyst is discussed in relation to the numbered steps of Figure 11. When the nanocomposite system is illuminated (1) with the HID light, both TiO_2 and CdS are activated and generate e^-_{cb} and h^+_{vb} in their respective conduction and valence bands (2). Because the condition band (CB) of CdS is at a more negative potential than that of TiO_2 [56], the electrons in the CB of CdS migrate across the interfacial boundary to the CB of TiO_2. Likewise, the photons generated in the valence band (VB) of TiO_2 which are at a more positive potential migrate to the VB of CdS which is at a less positive potential. The opposite migration of the generated charges step (3) facilitates charge carrier separation and thus reduces recombination rate [56, 57]. This ensures higher concentration of surface charges with sufficiently long lifetime to participate in redox reaction, thereby, imparting higher photocatalytic activities to the nanocomposites compared to the parent constituents.

The transferred electrons in the active sites of TiO_2 react with adsorbed O_2 to form superoxide (O_2^-) (4). The O_2^- reacts with hydrogen ion to form H_2O_2, which decomposes to hydroxyl [14]. On the other hand, the trapped CdS hole also reacts with adsorbed water and adsorbed MB molecule to generate •OH radicals and MB transformation products (5), respectively. The bulk hydroxyl radicals generated through the superoxide route and the trapped holes route react with the remaining bulk MB and any MB transformation products (TP) to produce simpler molecules (8).

4. Conclusion

In this work, visible light active CdS/TiO_2 nanocomposites containing various CdS content were successfully synthesized using microwave-assisted hydrothermal synthesis. The photocatalytic activities of the samples were studied using methylene blue as a model pollutant. From the results obtained, it is possible to draw the following conclusions:

(i) The nonlinear fits of adsorption data to Langmuir, Freundlich, and Freundlich-Langmuir (Sips) isotherms and to LPSO and PSO kinetic models indicate that the sorption of MB onto the parent TiO_2 and the CdS/TiO_2 nanocomposites obey the Sips model and PSO model, respectively.

(ii) Photocatalytic oxidation of MB was favorably predicted by apparent pseudo-first-order kinetics based on the Langmuir-Hinshelwood (L-H) model. Generally, the second-order adsorption rate (k_2) is about one order of magnitude higher than the apparent rate constants (k_a).

(iii) The photocatalytic results indicated that the Cd : Ti molar ratio has significant effect on the photodegradation of MB. Samples with low Cd : Ti content show 4-5 times more activity than that with high Cd : Ti content compared to activity of TiO_2.

Conflict of Interests

The authors declare that there is no conflict of interests regarding the publication of this paper.

Acknowledgment

The authors gratefully acknowledge the financial support provided by the Ministry of Education, Government of Malaysia, through Grant FGRS/1/11/TK/UPM/02/34, dated 1 August 2011, and RU Project Grant no. 05-02-12-2193RU.

References

[1] I. Khouni, B. Marrot, P. Moulin, and R. Ben Amar, "Decolourization of the reconstituted textile effluent by different process treatments: enzymatic catalysis, coagulation/flocculation and nanofiltration processes," *Desalination*, vol. 268, no. 1–3, pp. 27–37, 2011.

[2] A. K. Verma, R. R. Dash, and P. Bhunia, "A review on chemical coagulation/flocculation technologies for removal of colour from textile wastewaters," *Journal of Environmental Management*, vol. 93, no. 1, pp. 154–168, 2012.

[3] P. A. Pekakis, N. P. Xekoukoulotakis, and D. Mantzavinos, "Treatment of textile dyehouse wastewater by TiO_2 photocatalysis," *Water Research*, vol. 40, no. 6, pp. 1276–1286, 2006.

[4] V. J. P. Vilar, L. X. Pinho, A. M. A. Pintor, and R. A. R. Boaventura, "Treatment of textile wastewaters by solar-driven advanced oxidation processes," *Solar Energy*, vol. 85, no. 9, pp. 1927–1934, 2011.

[5] U. Wiesmann, I. S. Choi, and E.-M. Dombrowski, "Biodegradation of special organic compounds," in *Fundamentals of Biological Wastewater Treatment*, pp. 195–222, Wiley-VCH, Weinheim, Germany, 2006.

[6] M. A. Barakat, "New trends in removing heavy metals from industrial wastewater," *Arabian Journal of Chemistry*, vol. 4, no. 4, pp. 361–377, 2011.

[7] A. Hakki, R. Dillert, and D. W. Bahnemann, "Factors affecting the selectivity of the photocatalytic conversion of nitroaromatic compounds over TiO_2 to valuable nitrogen-containing organic compounds," *Physical Chemistry Chemical Physics*, vol. 15, no. 8, pp. 2992–3002, 2013.

[8] X. Yang, H. Cui, Y. Li, J. Qin, R. Zhang, and H. Tang, "Fabrication of Ag_3PO_4-graphene composites with highly efficient and stable visible light photocatalytic performance," *ACS Catalysis*, vol. 3, no. 3, pp. 363–369, 2013.

[9] X. Chen, C. Li, M. Grätzel, R. Kosteckid, and S. S. Mao, "Nanomaterials for renewable energy production and storage," *Chemical Society Reviews*, vol. 41, no. 23, pp. 7909–7937, 2012.

[10] R. W. Matthews, "An adsorption water purifier with in situ photocatalytic regeneration," *Journal of Catalysis*, vol. 113, no. 2, pp. 549–555, 1988.

[11] D. Chatterjee and S. Dasgupta, "Visible light induced photocatalytic degradation of organic pollutants," *Journal of Photochemistry and Photobiology C: Photochemistry Reviews*, vol. 6, no. 2-3, pp. 186–205, 2005.

[12] A. Fujishima, T. N. Rao, and D. A. Tryk, "Titanium dioxide photocatalysis," *Journal of Photochemistry and Photobiology C: Photochemistry Reviews*, vol. 1, no. 1, pp. 1–21, 2000.

[13] H. Park, Y. Park, W. Kim, and W. Choi, "Surface modification of TiO_2 photocatalyst for environmental applications," *Journal of Photochemistry and Photobiology C: Photochemistry Reviews*, vol. 15, no. 1, pp. 1–20, 2013.

[14] X. Li, T. Xia, C. Xu, J. Murowchick, and X. Chen, "Synthesis and photoactivity of nanostructured CdS–TiO_2 composite catalysts," *Catalysis Today*, vol. 225, pp. 64–73, 2014.

[15] T. T. D. Vu, F. Mighri, A. Ajji, and T.-O. Do, "Synthesis of titanium dioxide/cadmium sulfide nanosphere particles for photocatalyst applications," *Industrial and Engineering Chemistry Research*, vol. 53, no. 10, pp. 3888–3897, 2014.

[16] C. Li, J. Yuan, B. Han, L. Jiang, and W. Shangguan, "TiO_2 nanotubes incorporated with CdS for photocatalytic hydrogen production from splitting water under visible light irradiation," *International Journal of Hydrogen Energy*, vol. 35, no. 13, pp. 7073–7079, 2010.

[17] Y. J. Zhang, W. Yan, Y. P. Wu, and Z. H. Wang, "Synthesis of TiO_2 nanotubes coupled with CdS nanoparticles and production of hydrogen by photocatalytic water decomposition," *Materials Letters*, vol. 62, no. 23, pp. 3846–3848, 2008.

[18] S. Peng, Y. Huang, and Y. Li, "Rare earth doped TiO_2-CdS and TiO_2-CdS composites with improvement of photocatalytic hydrogen evolution under visible light irradiation," *Materials Science in Semiconductor Processing*, vol. 16, no. 1, pp. 62–69, 2013.

[19] W. Zhao, Z. Bai, A. Ren, B. Guo, and C. Wu, "Sunlight photocatalytic activity of CdS modified TiO_2 loaded on activated carbon fibers," *Applied Surface Science*, vol. 256, no. 11, pp. 3493–3498, 2010.

[20] L. Zhu, Z. da Meng, K. Youn Cho, and W. Chun Oh, "Synthesis of CdS/CNT-TiO_2 with a high photocatalytic activity in photodegradation of methylene blue," *New Carbon Mater*, vol. 27, no. 3, pp. 166–174, 2012.

[21] Z.-D. Meng, L. Zhu, J.-G. Choi, C. Y. Park, and W.-C. Oh, "Sonocatalytic degradation of Rhodamine B in the presence of C_{60} and CdS coupled TiO_2 particles," *Ultrasonics Sonochemistry*, vol. 19, no. 1, pp. 143–150, 2012.

[22] Y. Xie, G. Ali, S. H. Yoo, and S. O. Cho, "Sonication-assisted synthesis of CdS quantum-dot-sensitized TiO_2 nanotube arrays with enhanced photoelectrochemical and photocatalytic activity," *ACS Applied Materials and Interfaces*, vol. 2, no. 10, pp. 2910–2914, 2010.

[23] E. A. Kozlova, N. S. Kozhevnikova, S. V. Cherepanova et al., "Photocatalytic oxidation of ethanol vapors under visible light on CdS-TiO_2 nanocatalyst," *Journal of Photochemistry and Photobiology A: Chemistry*, vol. 250, pp. 103–109, 2012.

[24] G. Yang, B. Yang, T. Xiao, and Z. Yan, "One-step solvothermal synthesis of hierarchically porous nanostructured CdS/TiO_2 heterojunction with higher visible light photocatalytic activity," *Applied Surface Science*, vol. 283, pp. 402–410, 2013.

[25] B. Jiang, X. Yang, X. Li, D. Zhang, J. Zhu, and G. Li, "Core-shell structure CdS/TiO_2 for enhanced visible-light-driven photocatalytic organic pollutants degradation," *Journal of Sol-Gel Science and Technology*, vol. 66, no. 3, pp. 504–511, 2013.

[26] M. Baghbanzadeh, L. Carbone, P. D. Cozzoli, and C. O. Kappe, "Microwave-assisted synthesis of colloidal inorganic nanocrystals," *Angewandte Chemie—International Edition*, vol. 50, no. 48, pp. 11312–11359, 2011.

[27] Y. C. Zhang, J. Li, M. Zhang, and D. D. Dionysiou, "Size-tunable hydrothermal synthesis of SnS_2 nanocrystals with high performance in visible light-driven photocatalytic reduction of aqueous Cr(VI)," *Environmental Science and Technology*, vol. 45, no. 21, pp. 9324–9331, 2011.

[28] J. Tauc and A. Menth, "States in the gap," *Journal of Non-Crystalline Solids*, vol. 8–10, pp. 569–585, 1972.

[29] L. Zou, X. Xiang, J. Fan, and F. Li, "Single-source precursor to complex metal oxide monoliths with tunable microstructures and properties: the case of Mg-containing materials," *Chemistry of Materials*, vol. 19, no. 26, pp. 6518–6527, 2007.

[30] Y. P. Teoh, M. A. Khan, and T. S. Y. Choong, "Kinetic and isotherm studies for lead adsorption from aqueous phase on carbon coated monolith," *Chemical Engineering Journal*, vol. 217, pp. 248–255, 2013.

[31] J. Yu, L. Zhang, B. Huang, and H. Liu, "Synthesis of spherical TiO_2 made up of high reactive facets of (001)," *International Journal of Electrochemical Science*, vol. 8, no. 4, pp. 5810–5816, 2013.

[32] J. Luo, L. Ma, T. He et al., "TiO_2/(CdS, CdSe, CdSeS) nanorod heterostructures and photoelectrochemical properties," *Journal of Physical Chemistry C*, vol. 116, no. 22, pp. 11956–11963, 2012.

[33] S. Qian, C. Wang, W. Liu, Y. Zhu, W. Yao, and X. Lu, "An enhanced CdS/TiO_2 photocatalyst with high stability and activity: effect of mesoporous substrate and bifunctional linking molecule," *Journal of Materials Chemistry*, vol. 21, no. 13, pp. 4945–4952, 2011.

[34] C. J. Murphy and J. L. Coffer, "Quantum dots: a primer," *Applied Spectroscopy*, vol. 56, no. 1, pp. 16A–27A, 2002.

[35] A. Kubacka, M. Fernández-García, and G. Colón, "Advanced nanoarchitectures for solar photocatalytic applications," *Chemical Reviews*, vol. 112, no. 3, pp. 1555–1614, 2012.

[36] T. Huang and G. Jie, "Electrogenerated chemiluminescence of novel TiO_2/CdS nanocomposites for sensitive assays of cancer cells," *Analytical Biochemistry*, vol. 442, no. 1, pp. 34–39, 2013.

[37] K. Y. Foo and B. H. Hameed, "Insights into the modeling of adsorption isotherm systems," *Chemical Engineering Journal*, vol. 156, no. 1, pp. 2–10, 2010.

[38] G. McKay, H. S. Blair, and J. R. Gardner, "Adsorption of dyes on chitin. I. Equilibrium studies," *Journal of Applied Polymer Science*, vol. 27, no. 8, pp. 3043–3057, 1982.

[39] B. H. Hameed, A. T. M. Din, and A. L. Ahmad, "Adsorption of methylene blue onto bamboo-based activated carbon: kinetics and equilibrium studies," *Journal of Hazardous Materials*, vol. 141, no. 3, pp. 819–825, 2007.

[40] M. L. Fetterolf, H. V. Patel, and J. M. Jennings, "Adsorption of methylene blue and acid blue 40 on titania from aqueous solution," *Journal of Chemical and Engineering Data*, vol. 48, no. 4, pp. 831–835, 2003.

[41] L. Xiong, Y. Yang, J. Mai et al., "Adsorption behavior of methylene blue onto titanate nanotubes," *Chemical Engineering Journal*, vol. 156, no. 2, pp. 313–320, 2010.

[42] Z. C. Kadirova, K.-I. Katsumata, T. Isobe, N. Matsushita, A. Nakajima, and K. Okada, "Adsorption and photodegradation of methylene blue with Fe_2O_3-activated carbons under UV illumination in oxalate solution," *Journal of Environmental Chemical Engineering*, vol. 2, no. 4, pp. 2026–2036, 2014.

[43] R.-L. Tseng, F.-C. Wu, and R.-S. Juang, "Characteristics and applications of the Lagergren's first-order equation for adsorption kinetics," *Journal of the Taiwan Institute of Chemical Engineers*, vol. 41, no. 6, pp. 661–669, 2010.

[44] Y. S. Ho and G. McKay, "Sorption of dye from aqueous solution by peat," *Chemical Engineering Journal*, vol. 70, no. 2, pp. 115–124, 1998.

[45] N. K. Dey, M. J. Kim, K.-D. Kim et al., "Adsorption and photocatalytic degradation of methylene blue over TiO_2 films on carbon fiber prepared by atomic layer deposition," *Journal of Molecular Catalysis A: Chemical*, vol. 337, no. 1-2, pp. 33–38, 2011.

[46] N. Xu, Z. Shi, Y. Fan, J. Dong, J. Shi, and M. Z.-C. Hu, "Effects of particle size of TiO_2 on photocatalytic degradation of methylene blue in aqueous suspensions," *Industrial and Engineering Chemistry Research*, vol. 38, no. 2, pp. 373–379, 1999.

[47] R. Suresh, K. Giribabu, R. Manigandan et al., "Doping of Co into V_2O_5 nanoparticles enhances photodegradation of methylene blue," *Journal of Alloys and Compounds*, vol. 598, pp. 151–160, 2014.

[48] P. Yan, H. Jiang, S. Zang, J. Li, Q. Wang, and Q. Wang, "Sol-solvothermal preparation and characterization of (Yb, N)-codoped anatase-TiO_2 nano-photocatalyst with high visible light activity," *Materials Chemistry and Physics*, vol. 139, no. 2-3, pp. 1014–1022, 2013.

[49] I. K. Konstantinou and T. A. Albanis, "TiO_2-assisted photocatalytic degradation of azo dyes in aqueous solution: kinetic and mechanistic investigations: a review," *Applied Catalysis B: Environmental*, vol. 49, no. 1, pp. 1–14, 2004.

[50] M. J. Flannagan, "Subjective and objective aspecs of headlamp glare: effects of size and spectral power," Tech. Rep. UMTRI-99-36, University of Michigan Transportation Research Institute Library, University of Michigan, Ann Arbor, Mich, USA, 1999.

[51] P. Samokhvalov, M. Artemyev, and I. Nabiev, "Basic principles and current trends in colloidal synthesis of highly luminescent semiconductor nanocrystals," *Chemistry*, vol. 19, no. 5, pp. 1534–1546, 2013.

[52] P. Reiss, M. Protière, and L. Li, "Core/shell semiconductor nanocrystals," *Small*, vol. 5, no. 2, pp. 154–168, 2009.

[53] F. E. Osterloh, "Inorganic nanostructures for photoelectrochemical and photocatalytic water splitting," *Chemical Society Reviews*, vol. 42, no. 6, pp. 2294–2320, 2013.

[54] A. J. Cowan and J. R. Durrant, "Long-lived charge separated states in nanostructured semiconductor photoelectrodes for the production of solar fuels," *Chemical Society Reviews*, vol. 42, no. 6, pp. 2281–2293, 2013.

[55] A. B. Makama, A. Salmiaton, E. B. Saion, T. S. Y. Choong, and N. Abdullah, "Microwave-assisted synthesis of porous ZnO/SnS_2 heterojunction and its enhanced photoactivity for water purification," *Journal of Nanomaterials*, vol. 2015, Article ID 108297, 13 pages, 2015.

[56] W. Li, X. Cui, P. Wang, Y. Shao, D. Li, and F. Teng, "Enhanced photosensitized degradation of rhodamine B on CdS/TiO_2 nanocomposites under visible light irradiation," *Materials Research Bulletin*, vol. 48, no. 9, pp. 3025–3031, 2013.

[57] W. Wang, J. Wang, Z. Wang et al., "P-n junction CuO/$BiVO_4$ heterogeneous nanostructures: synthesis and highly efficient visible-light photocatalytic performance," *Dalton Transactions*, vol. 43, no. 18, pp. 6735–6743, 2014.